Empirical Force-Field Assessment: The Interplay Between Backbone Torsions and Noncovalent Term Scaling

ERIC J. SORIN, VIJAY S. PANDE
Department of Chemistry, Stanford University, Structural Biology Department and SSRL85, Stanford, California 94305-5080

Received 8 November 2004; Accepted 11 January 2005
DOI 10.1002/jcc.020208
Published online in Wiley InterScience (www.interscience.wiley.com).

Abstract: The kinetic and thermodynamic aspects of the helix-coil transition in polyalanine-based peptides have been studied at the ensemble level using a distributed computing network. This study builds on a previous report, which critically assessed the performance of several contemporary force fields in reproducing experimental measurements and elucidated the complex nature of helix-coil systems. Here we consider the effects of modifying backbone torsions and the scaling of noncovalent interactions. Although these elements determine the potential of mean force between atoms separated by three covalent bonds (and thus largely determine the local conformational distributions observed in simulation), we demonstrate that the interplay between these factors is both complex and force field dependent. We quantitatively assess the heliophilicity of several helix-stabilizing potentials as well as the changes in heliophilicity resulting from such modifications, which can "make or break" the accuracy of a given force field, and our findings suggests that future force field development may need to better consider effect that vary with peptide length. This report also serves as an example of the utility of distributed computing in analyzing and improving upon contemporary force fields at the level of absolute ensemble equilibrium, the next step in force field development.

 J Comput Chem 26: 682–690, 2005

Key words: AMBER; distributed computing; protein folding; molecular dynamics; Fs peptide

Introduction

Modeling protein structure, thermodynamics, and kinetics in atomistic detail is a challenging task not possible through contemporary quantum computation. Instead, classical force fields are the predominant models used by biophysical theorists. Such potentials allow for atomic scale simulation of small biopolymers in explicit solvent for increasingly longer time scales, and have been used to simulate several aspects of biomolecular dynamics including protein folding.[1] The current state of classical potentials, which includes several all-atom models, was strongly influenced by the work of Jorgensen and coworkers (OPLS-AA),[2] MacKerell et al. (CHARMM22),[3] and Cornell et al. (AMBER-94).[4] Although there have been several updates to, and incarnations of, the original AMBER-94 potential,[5–8] few are yet as widely used or as well understood as the Cornell et al. force field.

Although a number of high-profile reports have been published recently on large protein structural dynamics using this and other classical potentials,[9–11] extending the regime of applicability of such potentials, both spatially and temporally, requires an accurate understanding of the predictions of such force fields for model systems that have been studied in detail experimentally. Through such understanding, classical models may be improved to yield better agreement with experiment, thereby increasing the dependability and predictive power of all-atom simulations.

To increase the accuracy and utility of modern force fields it is also helpful to understand how simple components of classical force fields interact to determine the kinetics and thermodynamics that are extracted from simulation. A prime example of this is the interplay between torsion potentials and the scaling of 1-4 van der Waals (vdW) and 1-4 charge–charge (QQ) interactions (those between atoms separated by three covalent bonds), all of which contribute to the conformational preferences in local regions of biomolecules. Because proteins are complex physical systems, it is

Correspondence to: V. S. Pande; e-mail: pande@stanford.edu

Contract/grant sponsor: Veatch and Krell/DOE CGSF predoctoral fellowships (to E.J.S.)

Contract/grant sponsor: ACS-PRF; contract/grant number: 36028-AC4

Contract grant sponsor: NSF Molecular Biophysics

Contract/grant sponsor: NSF MRSEC CPIMA; contract/grant number: DMR-9808677

Contract/grant sponsor: Intel

necessary to first gain an understanding of these issues with respect to the most elementary of protein substructures. We thus focus on the helix-coil transition which, although having been studied extensively by experimentalists and theorists alike for several decades, continues to generate ongoing debate in the literature.

We have recently employed our global distributed computing network to take a step in this direction by simulating an ensemble of long trajectories to obtain the kinetics and equilibrium distributions for two helical peptides in all-atom detail under several AMBER force fields.[12] In that study, which reported nearly 4 ms of explicit solvent simulation time, the exact degree of heliophilicity and heliophobicity of several AMBER force fields was assessed, and we showed that a new variant of the AMBER-99 potential, denoted AMBER-99ϕ, was superior to other force fields at reproducing experimental thermodynamic and kinetic measurements for the 21-residue polyalanine-based F_s peptide. In this follow-up report, we focus on the three AMBER force fields in which helical conformations were stable to varying degrees, assessing the interplay between backbone torsion potentials and the scaling of 1-4 vdW and QQ interactions on the kinetics and equilibrium structural character predicted by these force fields for this model helix-coil system.

Methods

The capped F_s peptide (Ace-A_5[AAAR$^+$A]$_3$A-NMe) was simulated using the AMBER-94,[4] AMBER-GS,[7] and AMBER-99ϕ[12] all-atom potentials ported into the GROMACS molecular dynamics suite[13] as modified for the Folding@Home[14] infrastructure (http://folding.stanford.edu). The AMBER-GS force field of Garcia and Sanbonmatsu[7] is a variant of the AMBER-94 potential in which ϕ and ψ backbone torsions are removed from the potential. Additionally, standard AMBER 1-4 vdW scaling (multiplication by1/2 for these interactions) was also removed in this force field.[15,16] However, because several subsequent reports[1,12,17] used the nomenclature "AMBER-GS" to refer solely to the removal of backbone torsions, we maintain this nomenclature herein. The potential used in the studies of Garcia and coworkers[7,15,16] is thus referred to herein as "AMBER-GS-S." Although this potential was originally reported to fix the overstabilization of helical conformations in AMBER-94, we showed using ensemble simulations that this force field actually *increases* the heliophilicity inherent to the AMBER-94 potential. In contrast, the AMBER-99ϕ variant, which replaces the ϕ potential in the *heliophobic* AMBER-99 with that of AMBER-94, yields the best agreement with several experimental measurements.[12]

A canonical helix ($\phi = -57°$, $\psi = -47°$) and a random coil configuration with no helical content were generated and centered in 40 Å cubic boxes. Electroneutrality was gained by placing three Cl^- ions randomly around the solute with minimum ion–ion and ion–solute separations of 5 Å. The helix and coil conformations were then solvated with 2075 and 2065 TIP3P water molecules,[17] respectively. After energy minimization using a steepest descent algorithm, and solvent annealing for 500 ps of molecular dynamics (MD) with the peptide conformation held fixed, each of these conformations served as the starting point for 1000 independent MD trajectories in each AMBER potential, which were simulated on ~25,000 CPUs within the Folding@Home supercluster.

All simulations reported herein were conducted under NPT conditions[18] at 1 atm and 305 K, the approximate F_s midpoint temperature detected by circular dichroism[19] and ultraviolet resonance Raman.[20] Long-range electrostatic interactions were treated using the reaction field method with a dielectric constant of 80, and 9 Å cutoffs were imposed on all Coulombic and Lennard–Jones interactions. Nonbonded pair lists were updated every 10 steps, and covalent bonds involving hydrogen atoms were constrained with the LINCS algorithm.[21] An integration step size of 2 fs was used with coordinates stored every 100 ps.

Identical ensemble simulations were conducted in each force field (1) without the default AMBER scaling of 1-4 vdW interactions (denoted by the force field name suffix -S), (2) without the default AMBER scaling of 1-4 QQ interactions (-Q), and (3) with all 1-4 scaling turned off (-SQ). This study thus assesses twelve variants of the AMBER force field including four forms of the Cornell et al. force field (AMBER-94,[4] AMBER94-S, AMBER94-Q, and AMBER94-SQ), four forms of the modified version of Garcia & Sanbonmatsu (AMBER-GS,[7] AMBERGS-S, AMBERGS-Q, and AMBERGS-SQ), and four forms of our AMBER99 variant (AMBER99ϕ,[12] AMBER99ϕ-S, AMBER99ϕ-Q, AMBER99ϕ-SQ). This combination allows us to directly assess, from equilibrium helix-coil data, the affects of these modifications as well as the interplay between them. Table 1 summarizes the force field variants studied and the cumulative sampling achieved. A total sampling time of over 1.5 ms and a total equilibrium sampling of over 600 μs in TIP3P solvent, orders of magnitude longer than the ~16 ns folding time of F_s, is included in the following analyses.

As described in our previous report,[12] we follow the work of Garcia and coworkers, who used Lifson-Roig (LR) statistics[22] to assess helicity. In this model, residues are defined as helical if $\phi = -60(\pm 30)°$ and $\psi = -47(\pm 30)°$ and nonhelical otherwise, and we have shown previously that this is an adequate cutoff applied to the helical regime.[12] Using these cutoffs, a weight matrix for the central residue in the eight possible helix-coil conformational triplets is simplified as[22]

$$M = \begin{array}{c} \\ h\bar{h} \\ h\bar{c} \\ c(h \cup \bar{c}) \end{array} \begin{array}{c} \begin{array}{ccc} \bar{h}h & \bar{h}c & \bar{c}(h \cup c) \end{array} \\ \begin{pmatrix} w & v & 0 \\ 0 & 0 & 1 \\ v & v & 1 \end{pmatrix} \end{array}, \qquad (1)$$

where v and w are the LR nucleation and propagation constants, bars specify the central residue in the triplet, and $\cup$ represents the combined helical and nonhelical portion of the (ϕ,ψ) space. This leads to the molecular partition function

$$Z = (0 \quad 0 \quad 1)\, M'' \begin{pmatrix} 0 \\ 1 \\ 1 \end{pmatrix}, \qquad (2)$$

which was used to calculate the helical properties of our simulated ensembles. Namely, the mean number of helical hydrogen bonds is given by

Table 1. Force Fields Compared and Sampling Achieved.[a]

Force field	ϕ/ψ	vdW	QQ	Max (ns)	Total time (μs)	>EQ (μs)
AMBER-94	on	on	on	201	144.91	66.91
AMBER-94-S	on	off	on	130	127.15	28.00
AMBER-94-Q	on	on	off	120	105.84	31.49
AMBER-94-SQ	on	off	off	115	103.27	29.10
AMBER-GS	off	on	on	200	248.43	168.32
AMBER-GS-S	off	off	on	120	122.27	43.52
AMBER-GS-Q	off	on	off	115	105.68	31.43
AMBER-GS-SQ	off	off	off	105	105.70	31.90
AMBER-99ϕ	on	on	on	170	141.69	63.93
AMBER-99ϕ-S	on	off	on	115	124.03	45.00
AMBER-99ϕ-Q	on	on	off	110	104.26	30.39
AMBER-99ϕ-SQ	on	off	off	115	104.16	30.42
Total					1537.39	600.41

[a]Each force field was sampled using 1000 trajectories starting in the helix state and 1000 trajectories starting in the coil state, totaling 24,000 trajectories in all.

$$\langle N_h \rangle = \partial \ln Z / \partial \ln w \tag{3}$$

and the mean number of helical segments of two or more residues is given by

$$\langle N_s \rangle = \partial \ln Z / \partial \ln v_{12}, \tag{4}$$

where v_{12} is the v in the first row and second column of the weight matrix. The mean number of helical residues is related to these quantities by

$$\langle N \rangle = \langle N_h \rangle + 2\langle N_s \rangle. \tag{5}$$

Combining these relations thereby allows for the simultaneous evaluation of v and w for given values of $\langle N \rangle$ and $\langle N_s \rangle$, which are extracted from the simulated ensembles. To examine the effects of force field modifications, we also consider the largest number of contiguous helical residues in a given conformation, N_c.

Results and Discussion

Figure 1 demonstrates the convergence to equilibrium from the helix and coil states along the Lifson–Roig N and N_s metrics. The AMBER-94 and AMBER-99ϕ force fields rapidly equilibrate, and we choose 40 ns as a conservative starting point to consider the ensembles as equilibrated. As reported previously,[12] the AMBER-GS potential does not fully equilibrate on the 100 ns time scale. However, due to the degree of helicity present in those ensembles we can approximate the equilibrium properties for this potential as the lower bounds that result from using the same equilibrium starting point as chosen for the other force fields.

We consider two aspects of the free energy landscape for the helix-coil system under the force fields studied. Figure 2 displays free energy profiles for each force field variant projected onto the Ramachandran map and represents residue-level sampling for each potential. The free energy profile projected onto the radius of gyration (R_g) and LR statistics (N and N_c) in Figure 3 represents the molecular states present in the helix-coil equilibria, with changes that are interpreted as resulting from changes in the Ramachandran free energy plane. We also consider several experimental measurements in this comparative assessment of force-field accuracy, to which the equilibrium character predicted by each published and modified potential can be compared. As shown in Table 2, these include the LR thermodynamic parameters v and w, the coil-helix transition rate $k_{C\rightarrow H}$, the mean R_g, and the 3_{10} helical character $\langle \%3_{10} \rangle_{EQ}$. The equilibrium values for each modified force field in Table 2 include arrows representing the direction of shift away from the published force field that results upon each modification.

First and foremost, the total helicity N shows significant variation between the force fields. As reported previously,[12] we find that the removal of backbone torsions (AMBER-94 $\rightarrow$ AMBER-GS) results in an increased helical content of $\sim$50% to yield an ensemble of nearly ideal helical conformations. The mean number of helical segments simultaneously drops, being only slightly higher than 1 for the AMBER-GS potential. The stability of the α-helical regime ($\phi = -60°$, $\psi = -47°$) is easily identified in the free energy profiles of Figure 2: although there is a clear minimum in that region for AMBER-94 and AMBER-99ϕ, the basin for α-helical conformations in AMBER-GS is several kT levels deeper than these less heliophilic force fields, a feature that is not significantly altered by the removal of 1-4 scaling terms for AMBER-GS. As one might expect, ϕ/ψ torsions are the most definitive element of a given force field with respect to predicted helix-coil equilibria.

Interestingly, removal of 1-4 vdW scaling has varied effects. For AMBER-94, removing this term increases helicity by 5.5%, yet for AMBER-GS it *reduces* helicity by 3.8%. There is thus a nonadditive nature to the combination of backbone torsions and 1-4 vdW scaling. Additionally, the mean number of helical segments changes very little between scaled and unscaled ensembles, demonstrating that the primary effect of this term is to increase or decrease the propagation of helical segments rather than adding

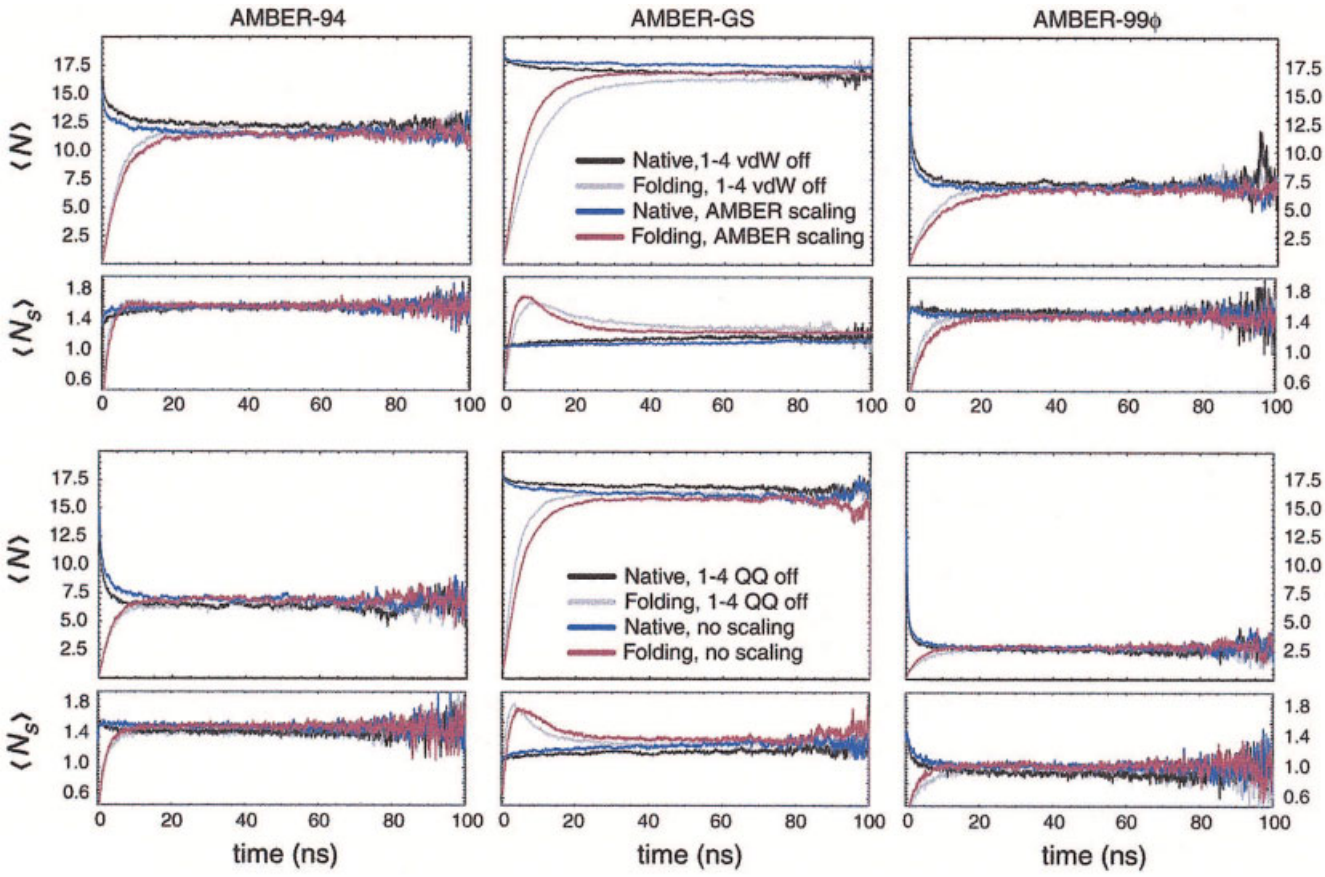

Figure 1. Time evolution of the F_s folding ensembles under the AMBER-94 (left), AMBER-GS (center), and AMBER-99ϕ (right) potentials including mean helical content, and mean number of helical segments per conformation according to classical LR counting theory. The top panels include curves for these potentials with standard AMBER scaling (red and blue) and with 1-4 vdW scaling removed (black and gray). The bottom panels include curves for these potentials with 1-4 QQ scaling turned off (black and gray) and with both 1-4 QQ and 1-4 vdW scaling turned off (red and blue).

stabilization to helix nuclei, as shown by the changes in v and w. In contrast, heliophilicity increases only slightly for the AMBER-99ϕ potential when scaling is removed. In comparing the three force fields, we thus see a myriad of behaviors when vdW scaling is removed. Notably, the most heliophilic force field (AMBER-GS) becomes less so, whereas the closest to experiment of the three (AMBER-99ϕ) shows the least sensitivity to this term. The calculated LR parameters are compared to the experimental values in Table 2. As we noted in our previous work,[12] this comparison is somewhat superficial due to the LR model and the artificial cutoffs placed on the helical regime of ϕ/ψ space, but offers a statistical comparison nonetheless.

In comparison, the removal of 1-4 QQ scaling results in a significant and uniform decrease in helicity in all force fields, with both nucleation and propagation parameters decreasing by roughly 20 to 35%. When both of these scaling terms are turned off, the removal of 1-4 QQ scaling dominates and the helicity decreases significantly. However, these terms are not additive: the result of removing both scaling terms in the AMBER-GS potential is slightly less significant than the removal of QQ scaling alone. As shown in the corresponding Ramachandran free energy maps for AMBER-GS (Fig. 2), these effects results from the broadening of nonhelical local minima and added stability of those states, whereas the profiles for AMBER-94 and AMBER-99ϕ show that the primary result is the slight destabilization of the helical regime.

It is also enlightening to consider changes in the folding kinetics upon force field modifications. The folding time for this peptide was determined to be ~16 ns by Williams et al. using a two-state model to fit Tjump infrared data,[23] thereby validating the prediction of Brooks using a master equation kinetic model that placed helix formation on the tens of nanoseconds (rather than microseconds) time scale.[24] In our previous work we showed that a simple exponential fit of the time-dependent probability of complete helix formation for the AMBER-99ϕ potential yielded a folding rate $k_{C\rightarrow H}$ that was in agreement with this experimental value. As shown in Table 2, the changes in folding rates show significant variation in dependence on backbone torsions and 1-4 term scaling. The folding rate for the AMBER-94 potential, which is the fastest folding force field, decreases to a more reasonable value when backbone torsions are removed (AMBER-94 → AMBER-GS). As was the case for helicity, changes in the folding rate upon removal of 1-4 vdW scaling are dependent on the base force field: the AMBER-94 rate remains unchanged, the AMBER-GS rate

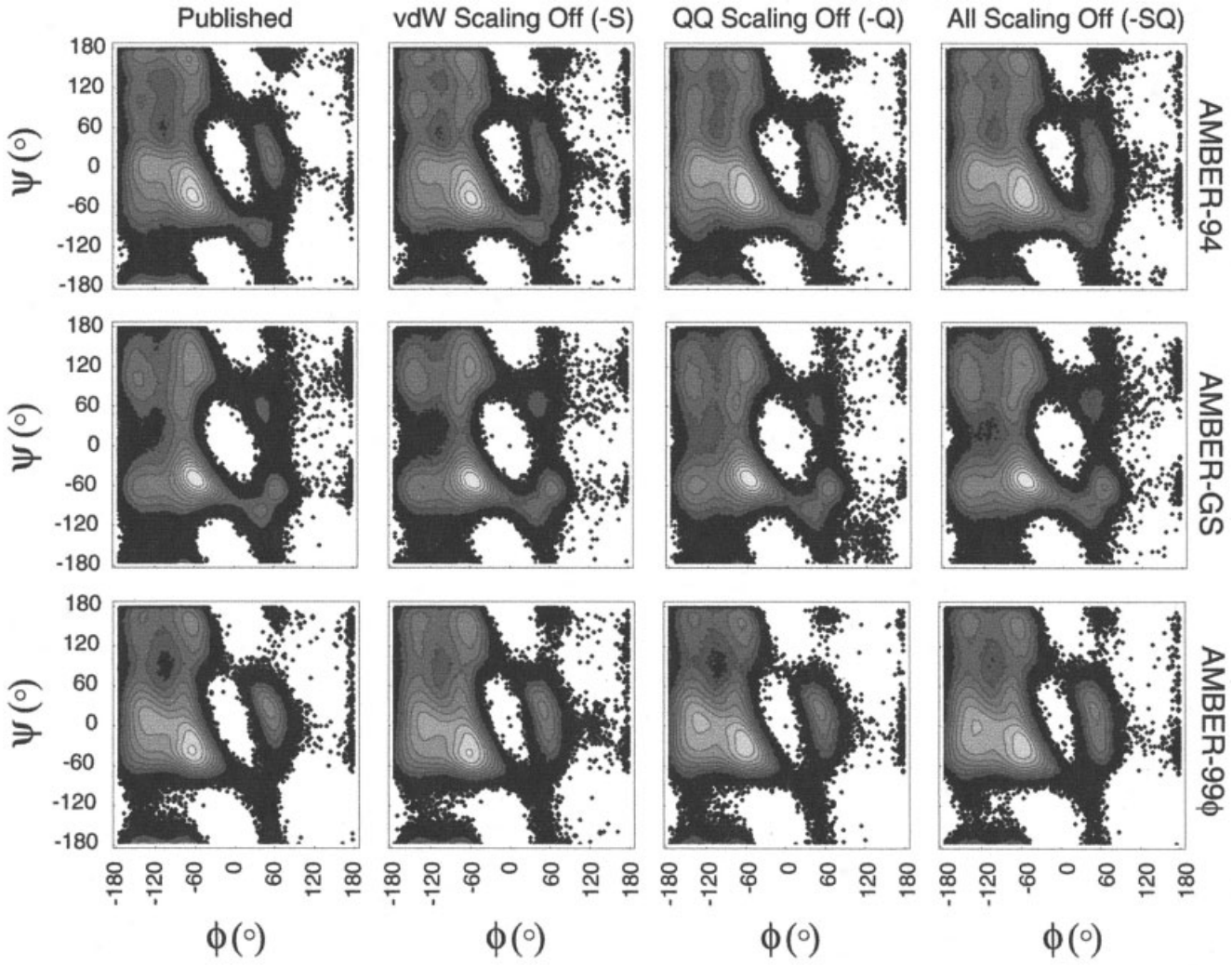

Figure 2. Free energy landscapes projected onto the Ramachandran map are shown for all variants of the three AMBER force fields studied including the published potentials, the -S potentials (with 1-4 van der Waals scaling turned off), the -Q potentials (with 1-4 electrostatic scaling turned off), and the -SQ potentials (with van der Waals and electrostatic scaling turned off). Each map consists of backbone torsional values binned in 3° intervals for all residues in ~40,000 equilibrium conformations, and contours represent kT units at 305 K.

decreases by a factor of 2, and the AMBER-99ϕ increases significantly. As with the comparisons of LR parameters above, the removal of 1-4 vdW scaling and backbone torsions shows a complex, nonadditive effect on the folding kinetics.

The removal of 1-4 QQ scaling is again more uniform, increasing the folding rate for each force field by 50% or more. Removal of both scaling factors, however, shows again the complex nature of the interactions between these force field elements. Although removal of 1-4 vdW scaling in AMBER-94 yields no change in the folding rate, and removal of 1-4 QQ speeds the transition by ~60%, the combined effect results in a folding rate that is only ~35% faster than when employing standard AMBER vdW and QQ scaling. In AMBER-GS the combined effect leaves the rate unchanged, and in AMBER-99ϕ the combination appears more additive, yielding a rate that is roughly four times faster than when employing standard AMBER scaling.

We can also compare the predicted R_g and 3_{10}-helix content of these ensembles as done in our previous work.[12] Because the LR theory does not differentiate between helical types (the 3_{10}-helix falls within the helical portion of the ϕ/ψ space), the Dictionary of Secondary Structure in Proteins[25] was used to evaluate 3_{10}-helix content. For each force field, removal of vdW scaling reduces the radius of gyration by roughly a quarter of an Angstrom, leaving the scaled AMBER-99ϕ result in best agreement with the value of ~9 Å extracted from small angle X-ray scattering (SAXS).[26] Removal of QQ scaling, on the other hand, results in changes in the mean R_g that depend on the force field, with AMBER-GS showing the largest sensitivity. Removal of both scaling terms also results in a uniform decrease in mean molecular size, yet once again demonstrates the nonadditive nature of these terms. Indeed, for the AMBER-99ϕ potential, the removal of both terms results in less overall effect that the removal of QQ scaling alone.

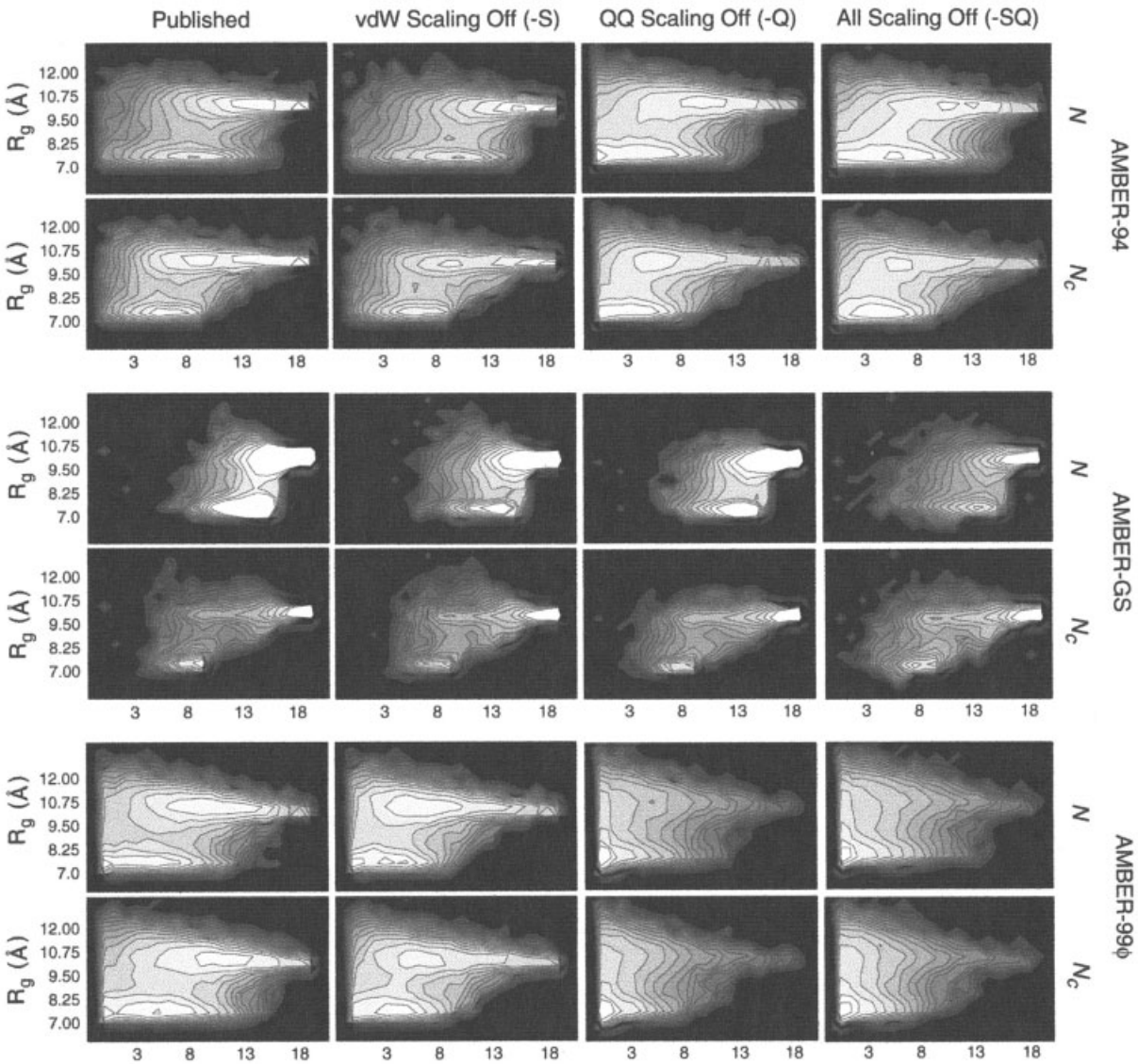

Figure 3. Free energy landscapes for F_s projected onto the radius of gyration R_g, number of helical residues N, and largest contiguous helical segment N_c for each force field variant studied. Each landscape was generated using ~40,000 peptide conformations randomly chosen from the equilibrium simulation ensembles (including folding and unfolding ensembles). Contours represent 0.25 kcal/mol intervals with each conformation assigned a statistical free energy $-RT\,\mathrm{Log}P$, where P is the probability of the conformation within the ensemble sampled. The radius of gyration was binned in 0.5 Å intervals for all plots.

The 3_{10}-helix content is highly sensitive to force field changes, as shown in Table 2. Removal of backbone torsion potentials from AMBER-94 diminishes the 3_{10} content to nearly zero regardless of vdW scaling. When backbone torsions are not removed, the removal of vdW scaling diminishes 3_{10}-helical character in the AMBER-94 and AMBER-99ϕ potentials by 31 and 16%, respectively. In contrast, removal of 1-4 QQ scaling uniformly increases 3_{10} content regardless of the potential, and the result of removing all AMBER scaling again has a nonadditive effect. As there is known to be significant 3_{10} character in helical polyalanine-based systems, particularly near the terminal regions,[12,27,28] the observed comparisons again show that AMBER-99ϕ outperforms these other helix-stabilizing force fields and also suggests that vdW scaling is an essential component in the AMBER family of force fields. Without this factor, a bias in the equilibrium conformational distribution is introduced that detracts from the 3_{10} character of the ensemble and enhances the sampling of the α-helical regime.

Because polyproline (PP) structure has been suggested as a dominant conformational form in the unfolded state of proteins, and some reports have assessed PP character in polyalanine peptides,[29–33] Table 2 also lists the equilibrium PP content for each equilibrium ensemble. The numbers shown in the table follow the

Table 2. Equilibrium Helix-Coil Properties for Scaled and Unscaled Helix-Coil Ensembles.[a]

Metric	Published	1–4 vdW not scaled (−S)	1–4 QQ not scaled (−Q)	No vdW or QQ scaling (−SQ)	Exp.
AMBER-94					
v	0.36	0.38 −	0.25 ↓	0.28 ↓	0.036
w	1.67	1.76 ↑	1.23 ↓	1.28 ↓	1.3
$k_{C\rightarrow H}(ns^{-1})$	0.11	0.11 −	0.18 ↑	0.15 ↑	0.06
$\langle R_g(Å)\rangle_{EQ}$	9.40	9.16 ↓	8.93 ↓	8.82 ↓	∼9*
$\langle \%3_{10}\rangle_{EQ}$	6.58	4.55 ↓	12.70 ↑	10.01 ↑	∼16%
$\langle \%PP\rangle_{EQ}$	1.93	2.41 ↑	1.71 ↓	2.32 ↑	—
AMBER-GS					
v	0.70	0.58 ↓	0.57 ↓	0.60 ↓	0.036
w	3.70	3.02 ↓	3.04 ↓	3.08 ↓	1.3
$k_{C\rightarrow H}(ns^{-1})$	0.08	0.04 ↓	0.13 ↑	0.08 −	0.06
$\langle R_g(Å)\rangle_{EQ}$	9.55	9.37 ↓	9.41 ↓	9.32 ↓	∼9[b]
$\langle \%3_{10}\rangle_{EQ}$	0.04	0.04 −	0.13 ↑	0.11 ↑	∼16%
$\langle \%PP\rangle_{EQ}$	2.39	3.40 ↑	2.18 ↓	2.94 ↑	—
AMBER-99ϕ					
v	0.26	0.28 −	0.17 ↓	0.17 ↓	0.036
w	1.26	1.29 −	0.96 ↓	0.96 ↓	1.3
$k_{C\rightarrow H}(ns^{-1})$	0.05	0.08 ↑	0.10 ↑	0.21 ↑	0.06
$\langle R_g(Å)\rangle_{EQ}$	9.24	9.02 ↓	8.72 ↓	8.80 ↓	∼9*
$\langle \%3_{10}\rangle_{EQ}$	17.84	14.92 ↓	21.30 ↑	18.07 ↑	∼16%
$\langle \%PP\rangle_{EQ}$	1.40	2.23 ↑	1.04 ↓	1.58 ↑	—

[a]Arrows for S, Q, and SQ ensemble values indicate direction of significant shifts from published force field values (which include standard AMBER scaling).
[b]Measured at ∼283 K.

analysis of Garcia,[16] which treats PP-coil statistics in a similar fashion to the LR theory described above. As shown in Table 2, PP conformations (near $\phi = -75°$, $\psi = 145°$) make up only a small portion of the sampled equilibria, as predicted from previous simulations[34] in the equilibrium limit using the CHARMM[35] potential and a continuum representation of the solvent. Both the removal of backbone torsions and the removal of 1-4 vdW scaling significantly increase the equilibrium PP content predicted by these force fields. Removal of backbone torsions in AMBER-94 increases PP content by 24%, while removing vdW scaling does so by 42%. The combined effect of these modifications, as employed in Garcia's work on helical polyalanine peptides,[7,15,16] increases PP content by 77% over the original Cornell potential, resulting from the stability gain of the PP region shown in Figure 2. In comparison, the PP content is increased by 59% in AMBER-99ϕ when vdW scaling is removed, and the increase in both this potential and AMBER-94 result not from added energetic stability, but from a broadening of the PP regime of the Ramachandran map.

The removal of 1-4 QQ scaling is once more relatively uniform, slightly detracting from PP content in each force field, which results from slight energetic destabilization and narrowing of the PP free energy basins shown in Figure 2. The role of vdW scaling is clearly prevalent in determining PP content however, and the combined effect of removing both scaling terms consistently results in a significant increase in PP content in comparison to the force fields when standard AMBER scaling is employed.

We note that the values reported in Table 2 represent equilibrium PP content, rather than PP content of the unfolded state, as was reported previously.[12] Although no experimental PP analysis has been conducted on this system, the general trends observed offer insight into the performance of these force fields as applied to model polyalanine-based systems. Interestingly, Shi et al. offered convincing evidence that the polyalanine A_7 peptide, blocked by two charged hydrophilic residues at each terminus, adopts a predominantly PP structure at biologically relevant temperatures with little helical structure (10% or less).[32] Zagrovic et al. have studied this same 7-mer peptide using SAXS alongside ensemble simulations similar to those described herein and found that even the best of these helix-coil force fields predict an overabundance of helical structure and little PP content in comparison to the experimental results.[36] This suggests that the accuracy of a given force field in reproducing the experimental observables for simple model systems (in this case, polyalanine-based peptides) is strongly influenced by peptide length, as noted in our previous work,[12] thus presenting an interesting and challenging new aspect of protein simulation for the computational community to consider.

Conclusion

Modern biomolecular mechanics force fields are known to suffer from many issues, and significant sampling has not been previously achieved using most commonly employed potentials to allow for a critical assessment of the ensemble level equilibrium predictions of these potentials. We have taken the next step in this direction, using distributed computing resources to obtain absolute

equilibrium sampling of a model helix-coil system, the most fundamental subclass of protein structural dynamics, allowing for such an assessment of the efficacy of each force field according to several experimentally characterized kinetic and thermodynamic properties. With this report we begin investigations of how individual force-field elements, and the interplay between them, play a role in determining the accuracy of a given potential with respect to the model helix-coil system, illustrating the utility of distributed computing architectures in allowing ample sampling for such analysis on the ensemble level.

As one might expect, backbone torsional potentials and 1-4 term scaling, which act collectively to determine the preferred conformational regions of the ϕ/ψ space sampled, strongly determine the helical properties of polyalanine-based peptides *in silico*. Indeed, the interplay between these elements is complex and not easily predicted *a priori*, and together these factors can "make or break" a given potential with respect to simple helical systems. Our results demonstrate how these factors influence helical content individually and in tandem. Removing backbone torsions from the Cornell et al. force field increases the overstabilization of helical conformations inherent to that potential and increases the sampling of polyproline structure. Removing 1-4 vdW scaling has similar effects unless backbone torsions are also removed, wherein the overstabilization of helical structure is not as significant, and polyproline structure is favored to a greater degree. This modification also yields lower 3_{10} helical character, an undesirable consequence. The removal of 1-4 QQ scaling uniformly decreases heliophilicity, molecular size, and PP content, while increasing the coil $\rightarrow$ helix transition rate and 3_{10}-helical character predicted by each force field.

These comparisons add insight to our understanding of how to best model helix-coil systems, and again show that the AMBER-99ϕ potential best reproduces experimental measurements on this system. Additionally, our results with this system and the smaller blocked A_7 peptide, in conjunction with the studies of Zaman et al. on alanine dimers and trimers,[37] suggest that a dependence of force field accuracy on peptide length exists even for simple, model polyalanine-based systems. It is intriguing to consider, particularly in light of the mean helix length of eight residues observed in naturally occurring soluble proteins, that moving from 3 to 7 to 21 ALA residues could yield such significant structural variation based solely on the length of the peptide. This observation, of course, adds yet another challenge to be tackled by the biosimulation community.

Indeed, additional studies are needed to better understand, on a quantitative basis, the factors that affect the accuracy and applicability of contemporary force fields with respect to the simulation of nontrivial systems ranging from small peptides to larger proteins. For instance, the various methods of evaluating electrostatic energies and forces (i.e., reaction field treatment and Ewald sum methods) may impact the predictions of helix-coil equilibrium and dynamics observed. Additionally, the lack of accurate temperature-dependent helix-coil equilibria predicted by these force fields,[12] alongside our recent observation of water model-dependent helix-coil equilibria (Sorin & Pande, in preparation), suggests that our understanding of specific elements of these potentials, such as those considered in this article, must include consideration of the solvation model employed.

Acknowledgments

We thank Young Min Rhee and Bojan Zagrovic for their critical reading of this manuscript, and members of the Pande Group and Angel Garcia for invaluable discussion. This work would not have been possible without the worldwide Folding@Home and Google Compute volunteers who contributed invaluable processor time (http://folding.stanford.edu).

References

1. Rhee, Y. M.; Sorin, E. J.; Jayachandran, G.; Lindahl, E.; Pande, V. S. Proc Natl Acad Sci USA 2004, 101, 6456.
2. Jorgensen, W. L.; Maxwell, D. S.; Tirado–Rives, J. J Am Chem Soc 1996, 118, 11225.
3. MacKerell, A. D., Jr.; Bashford, D.; Bellott, M.; Dunbrack, R. L., Jr.; Evanseck, J. D.; Field, M. J.; Fischer, S.; Gao, J.; Guo, H.; Ha, S.; Joseph–McCarthy, D.; Kuchnir, L.; Kuczera, K.; Lau, F. T. K.; Mattos, C.; Michnick, S.; Ngo, T.; Nguyen, D. T.; Prodhom, B.; Reiher, W. E., III; Roux, B.; Schlenkrich, M.; Smith, J. C.; Stote, R.; Straub, J.; Watanabe, M.; Wiórkiewicz–Kuczera, J.; Yin, D.; Karplus, M. J Phys Chem B 1998, 102, 3586.
4. Cornell, W. D.; Cieplak, P.; Bayly, C. I.; Gould, I. R.; Merz, K. M.; Ferguson, D. M.; Spellmeyer, D. C.; Fox, T.; Caldwell, J. W.; Kollman, P. A. J Am Chem Soc 1995, 117, 5179.
5. Kollman, P.; Dixon, R.; Cornell, W.; Fox, T.; Chipot, C.; Pohorille, A. In Computer Simulations of Biomolecular Systems: Theoretical and Experimental Applications; van Gunsteren, W. F.; Wiener, P. K., Eds.; Escom, Dordrecht, 1997, p. 83.
6. Wang, J.; Cieplak, P.; Kollman, P. A. J Comp Chem 2000, 21, 1049.
7. Garcia, A. E.; Sanbonmatsu, K. Y. Proc Natl Acad Sci USA 2001, 99, 2782.
8. Duan, Y.; Wu, C.; Chowdhury, S.; Lee, M. C.; Xiong, G.; Zhang, W.; Yang, R.; Cieplak, P.; Luo, R.; Lee, T.; Caldwell, J.; Wang, J.; Kollman, P. J Comp Chem 2003, 24, 1999.
9. Duan, Y.; Kollman, P. A. Science 1998, 282, 740.
10. Mayor, U.; Guydosh, N. R.; Johnson, C. M.; Grossmann, J. G.; Sato, S.; Jas, G. S.; Freund, S. M. V.; Alonsok, D. O. V.; Daggett, V.; Fersht, A. R. Nature 2003, 421, 863.
11. Zhou, R.; Huang, X.; Margulis, C. J.; Berne, B. J. Science 2004, 305, 1605.
12. Sorin, E. J.; Pande, V. S. Biophys J 2004, 88, in press.
13. Lindahl, E.; Hess, B.; van der Spoel, D. J Mol Mod 2001, 7, 306.
14. Zagrovic, B.; Sorin, E. J.; Pande, V. J Mol Biol 2001, 313, 151.
15. Nymeyer, H.; Garcia, A. E. Proc Natl Acad Sci USA 2003, 100, 13934.
16. Garcia, A. E. Polymer 2004, 45, 669.
17. Jorgensen, W. L.; Chandrasekhar, J.; Madura, J. D.; Impey, R. W.; Klein, M. L. J Chem Phys 1983, 79, 926.
18. Berendsen, H.; Postma, J.; Vangunsteren, W.; Dinola, A.; Haak, J. J Chem Phys 1984, 81, 3684.
19. Thompson, P. A.; Eaton, W. A.; Hofrichter, J. Biochemistry 1997, 36, 9200.
20. Ianoul, A.; Mikhonin, A.; Lednev, I. K.; Asher, S. A. J Phys Chem A 2002, 106, 3621.
21. Hess, B.; Bekker, H.; Berendsen, H. J. C.; Fraaije, J. G. E. M. J Comp Chem 1997, 18, 1463.
22. Qian, H.; Schellman, J. A. J Phys Chem 1992, 96, 3987.
23. Williams, S.; Causgrove, T. P.; Gilmanshin, R.; Fang, K. S.; Callender, R. H.; Woodruff, W. H.; Dyer, R. B. Biochemistry 1996, 35, 691.
24. Brooks, C. L. J Phys Chem 1996, 100, 2546.

25. Kabsch, W.; Sander, C. Biopolymers 1983, 22, 2577.
26. Zagrovic, B.; Jayachandran, G.; Millett, I. S.; Doniach, S.; Pande, V. S. 2004, in preparation.
27. Millhauser, G. L.; Stenland, C. J.; Hanson, P.; Bolin, K. A.; van de Ven, F. J. M. J Mol Biol 1997, 267, 963.
28. Armen, R.; Alonso, D. O. V.; Daggett, V. Protein Sci 2003, 12, 1145.
29. Drozdov, A. N.; Grossfield, A.; Pappu, R. V. J Am Chem Soc 2003, 126, 2574.
30. Kentsis, A.; Mezei, M.; Gindin, T.; Osman, R. Proteins 2004, 55, 493.
31. Mezei, M.; Fleming, P. J.; Srinivasan, R.; Rose, G. D. Proteins 2004, 55, 502.
32. Shi, Z.; Olson, C. A.; Rose, G. D.; Baldwin, R. L.; Kallenbach, N. R. Proc Natl Acad Sci USA 2002, 99, 9190.
33. Weise, C. F.; Weisshaar, J. C. J Phys Chem B 2003, 107, 3265.
34. Ohkubo, Y. Z.; Brooks, C. L. Proc Natl Acad Sci USA 2003, 100, 13916.
35. Brooks, B. R.; Bruccoleri, R. E.; Olafson, B. D.; States, D. J.; Swaminathan, S.; Karplus, M. J Comp Chem 1983, 4, 187.
36. Zagrovic, B.; Sorin, E. J.; Millett, I. S.; van Gunsteren, W. F.; Doniach, S.; Pande, V. S., Proc Natl Acad Sci USA 2005, to be published.
37. Zaman, M. H.; Shen, M.-Y.; Berry, R. S.; Freed, K. F.; Sosnick, T. R. J Mol Biol 2003, 331, 693.